

Modifying H^- resonance asymmetries with short light pulses

Jakob Bengtsson and Eva Lindroth

Department of Physics Stockholm University, AlbaNova University Center, SE-106 91 Stockholm, Sweden

(Received 26 March 2012; published 11 May 2012)

We present a method based on time-dependent perturbation theory and complex rotation to treat the interaction of a short light pulse with a correlated atomic system. The pulse is built from two short and weak pulses with Gaussian envelopes that are centered at two different frequencies. The method is applied to the negative hydrogen ion in the vicinity of a doubly excited resonance and it is shown that the two light pulses can be used to alter the Fano profile of a resonance.

DOI: [10.1103/PhysRevA.85.053413](https://doi.org/10.1103/PhysRevA.85.053413)

PACS number(s): 32.80.Rm, 31.15.-p, 32.70.Jz, 32.80.Gc

I. INTRODUCTION

The ability to create light pulses with subfemtosecond duration has opened the possibility to study electronic processes, such as ionization and charge transfer, on the same time scale at which the electronic wave packets evolve. Such processes often involve the formation of metastable, multiply excited states as crucial intermediate steps. These metastable *resonance* states decay further on a time scale that is typically comparable to the characteristic time evolution of the electronic wave packet itself. The description of population and decay of resonance states is decisive for the understanding and eventually controlling electron dynamics in many-electron systems.

Although resonances are reminiscent of stationary states, they are not eigenstates of any Hermitian Hamiltonian. Characterized by a large local component that delocalize with a finite rate, resonances can be defined as solutions to the Schrödinger equation with asymptotically outgoing behavior [1]. One way to enforce such boundary conditions is provided by the method of complex scaling (or complex rotation) [2–5]. It is based on a continuation of the radial variable into the complex plane and the resonances are found as eigenstates, with complex eigenvalues, to the complex rotated non-Hermitian Hamiltonian [6–17]. Identification and characterization of a resonance, in terms of energy position and lifetime, can now be made directly from its eigenvalue. In previous studies [18,19] we have explored the possibility to use uniform complex scaling also in connection with time-dependent problems. The purpose of the present study is to take advantage of the direct representation of the resonant states as an integral part of the energy spectrum to study atoms interacting with short light pulses. In particular, we are interested in how the photoelectron spectrum in the vicinity of a metastable state can be altered by the pulse.

Today's time-domain measurements of electron dynamics typically use attosecond-long short-wavelength pulses to initiate an event and femtosecond infrared laser fields to probe the outcome (see, e.g., Refs. [20–22]). The modeling of such experiments requires, due to the strength of the infrared field, the solution of the time-dependent Schrödinger equation (TDSE) (see, e.g., [23–27]). Direct integration of the TDSE in the presence of a time-varying light field is a computationally heavy undertaking for any system beyond hydrogen. Presently, such calculations can only be performed for few-electron

systems [25,28] or for slightly more complicated systems after a careful selection of which many-electron effects to include [27]. The strong infrared laser field also complicates the analysis of both experimental and theoretical investigations and hopefully it will be possible to use less intrusive pulses in future experiments, such that the light-matter interaction can be treated within perturbation theory. It is this situation which is addressed here. We consider two weak light pulses centered at two different frequencies but overlapping in both time and space and treat the interaction with the atomic system to second order in the light field.

The strong localization of a resonance state implies typically large transition matrix elements from the ground state and through, for example, photoabsorption, a substantial transfer of population from the ground state to the excited resonance state can thus take place. The subsequent decay of the excited state occurs usually predominately through emission of Auger electrons, resulting in a pronounced peak in the electron spectrum. Since ionization in the same channel is also possible through photoabsorption directly to the continuum from the ground state (i.e., without passing through the resonance), the two paths to ionization can interfere, thereby giving rise to the typical asymmetric Fano profiles [29]. The appearance of asymmetric line profiles is an interesting manifestation of quantum interference, which is found for different scattering processes and in a variety of quantum systems [30]. Since it is destructive (or constructive) interference between the paths that leads to the minimum (or maximum) in the probability of the process considered, ability to control these paths opens for a possibility to control the quantum process itself. Combined with tunability (e.g., through external fields), Fano resonances have indeed been discussed as a way to control, for example, quantum transport through quantum wires [31] or across Bose-Einstein condensates in optical lattices [32]. In photoionization, short light pulses give, in contrast to continuous monochromatic light sources, a possibility to influence the quantum paths and thereby the asymmetry of the Fano profiles, and this even in the weak-field limit. The purpose of the present study is to investigate this in more detail, and as an interesting test system we use H^- .

As is often the case for negative ions, the ground state of H^- is its only bound state. In contrast, the ion has a rich spectrum of resonances, with a series of resonances converging to the excited-state thresholds of the neutral system. The binding relative to each threshold is provided by the dipole potential

induced by the extra electron through mixing of the degenerate excited states in the atom. H^- resonances are thus strongly affected by electron correlation. The odd parity 1P resonances, which can be reached by one-photon absorption from the ground state, have been subjected to careful experimental studies (see Refs. [33,34] and references therein). Two-photon above-threshold detachment has further been used to study the lowest even parity 1D resonance [35,36], and calculations of multiphoton detachment rates with monochromatic light have been presented by several authors [37–39]. The focus of the present study is different. We study instead the effect of a light field localized in time, but with a broad spectral composition.

In Sec. II we briefly review some properties of uniform complex scaling and in Sec. III we outline the basis for time-dependent perturbation theory concentrating on how it is to be combined with complex rotation. The representation of the correlated field-free states is discussed in Sec. IV, while the results are discussed in Sec. V.

II. COMPLEX SCALING

Uniform complex scaling is based on the transformation

$$r \rightarrow r e^{i\theta}, \quad (1)$$

where r is the radial variable and θ the scaling angle, $0 < \theta < \pi/4$. The transformation yields a scaled non-Hermitian Hamiltonian: $H^\theta(\mathbf{r}) \equiv H(\mathbf{r} \exp(i\theta))$ with, generally, complex eigenvalues. However, bound eigenstates retain their real eigenenergies, and for these states the rotation can be seen just as a variable transformation. Resonance states, which could not have been described by a Hermitian Hamiltonian, will now appear. Such states have complex eigenvalues that are independent of (a sufficiently large) θ , and the imaginary parts are connected to decay rates as $\Gamma = 2|\text{Im}(E)|$. The continuum solutions, on the other hand, will have complex energies, with an argument determined by θ , $E \rightarrow E \exp(-i2\theta)$. In the following we will assume that we have a suitable representation of the space spanned by $H^\theta(\mathbf{r})$ in a finite basis, but the discussion of this basis is postponed until Sec. IV.

The form of the inner product is of special importance when complex rotation is used. The left eigenvectors can then no longer be constructed as the complex conjugate transpose of the right eigenvectors. As has been discussed (e.g., in Refs. [18,40]), the left eigenvectors to a Hamiltonian rotated by θ are instead identical to the complex conjugate transpose of the right eigenvectors to the same Hamiltonian rotated by $-\theta$. For the special case of a complex symmetric Hamiltonian matrix (e.g., the one representing the time-independent atomic Hamiltonian), this gives that the left eigenvectors are just the transpose of the right eigenvectors. When calculating different physical quantities with complex scaling, one generally has to treat matrix elements $\langle f | \hat{O} | i \rangle$ and $\langle i | \hat{O} | f \rangle$ separately, since the latter is no longer the complex conjugate of the former. Below we will first detail the expressions that are needed in a conventional Hermitian formulation and then outline the translation to the complex rotated case for each matrix element.

A. Energy distribution

The object of interest here is the energy distribution,

$$\frac{dP(\epsilon)}{d\epsilon} \equiv \langle \Psi | \Phi(\epsilon) \rangle \langle \Phi(\epsilon) | \Psi \rangle, \quad (2)$$

above the ionization threshold of the system after its exposure to an electromagnetic pulse. In Eq. (2), $\Phi(\epsilon)$ refers to the electronic state with energy ϵ . Above the first- but below the second-ionization threshold the photoelectron spectrum is directly given by $dP/d\epsilon$. For the calculation of the energy distribution we may use that

$$\langle \Psi | \Phi(\epsilon) \rangle \langle \Phi(\epsilon) | \Psi \rangle = \frac{1}{\pi} \text{Im} \left(\int \frac{\langle \Psi | \Phi(E_n) \rangle \langle \Phi(E_n) | \Psi \rangle}{E_n - \epsilon - i\gamma} dE_n \right), \quad (3)$$

where $\gamma \rightarrow 0^+$ and the integral runs over the continuum of nonbound energy states. The equivalence between the left- and right-hand side of Eq. (3) follows from the definition of the delta function as the limit

$$\delta(E_n - \epsilon) = \frac{1}{\pi} \lim_{\gamma \rightarrow 0^+} \frac{\gamma}{(E_n - \epsilon)^2 + \gamma^2}. \quad (4)$$

Now, with complex scaling, the corresponding expression is [18,41,42]

$$\frac{dP(\epsilon)}{d\epsilon} = \frac{1}{\pi} \text{Im} \left(\sum_n \frac{\langle \Psi^\theta | \Phi_n^\theta \rangle \langle \Phi_n^\theta | \Psi^\theta \rangle}{E_n^\theta - \epsilon} \right), \quad (5)$$

where $\langle \Psi^\theta |$ denotes the left state vector, and $|\Phi_n^\theta\rangle$ and $\langle \Phi_n^\theta|$ are the right and left eigenvectors to a suitable Hamiltonian $H^\theta(\mathbf{r})$ with eigenvalues E_n^θ . The complex energies E_n^θ allow us to replace the integration in Eq. (3) with a coherent discrete sum over pseudocontinuum and resonance states. Hence, $dP/d\epsilon$ can be retrieved without the construction of the actual electronic state with (real) energy ϵ . We note here also that, since $\text{Im}(E_n^\theta) < 0$, the denominator in Eq. (5) has a pole in the lower complex half plane, just as is the case for Eq. (3) when $\gamma \rightarrow 0^+$. The relation in Eq. (5) is a key expression in the present study and will be explored in more detail below. First, however, we will focus on the procedure to find the state vector after the laser pulse.

III. TIME-DEPENDENT PERTURBATION THEORY

For laser pulses in the weak-field regime, an excited wave packet can be calculated using standard time-dependent perturbation theory. The required formalism can be found in several textbooks (see, e.g., [43]), but it will nevertheless be briefly outlined here as a precursor for the transition to the complex scaled case.

Starting with the time-dependent Schrödinger equation

$$i\hbar \frac{\partial}{\partial t} \Psi(\mathbf{r}, t) = H(\mathbf{r}, t) \Psi(\mathbf{r}, t), \quad (6)$$

we divide the Hamiltonian into a time-independent and a time-dependent part, $H(t) = H_0 + H_I(t)$. By setting

$$\Psi(\mathbf{r}, t) = e^{-iH_0 t/\hbar} \tilde{\Psi}(\mathbf{r}, t), \quad (7)$$

and inserting it into Eq. (6), we arrive at the Schrödinger

equation in the interaction picture

$$i\hbar \frac{\partial}{\partial t} \tilde{\Psi}(\mathbf{r}, t) = e^{iH_0 t/\hbar} H_I(\mathbf{r}, t) e^{-iH_0 t/\hbar} \tilde{\Psi}(\mathbf{r}, t). \quad (8)$$

For a system initially prepared in the ground state, Φ_0 , the right state vector is expanded in the series

$$|\tilde{\Psi}\rangle = |\Phi_0\rangle + \sum_{m=1}^{\infty} |\tilde{\Psi}_m\rangle, \quad (9)$$

and similarly for the left state vector. The subscript m in Eq. (9) denotes the order of the expansion. $H_I(t)$ describes the interaction between the atom and the light field, which for an N -electron system in the dipole approximation and velocity gauge, reads

$$H_I(t) = \frac{e}{m} \mathbf{A}(t) \cdot \sum_{i=1}^N \mathbf{p}_i = \mathbf{A}(t) \cdot \mathbf{P}, \quad (10)$$

where capital \mathbf{P} is introduced to indicate the sum over the single-particle operators \mathbf{p}_i . We have also allowed the constant e/m to be absorbed in \mathbf{P} . The light is further assumed to be linearly polarized along the z direction $\mathbf{A}(t) = A(t)\hat{\mathbf{z}}$. From Eq. (8) the m th-order term $\tilde{\Psi}_m$ is now found as the solution to

$$i\hbar \frac{\partial}{\partial t} |\tilde{\Psi}_m\rangle = A(t) e^{iH_0 t/\hbar} P_z e^{-iH_0 t/\hbar} |\tilde{\Psi}_{m-1}\rangle, \quad (11)$$

$$-i\hbar \frac{\partial}{\partial t} \langle \tilde{\Psi}_m| = A(t) \langle \tilde{\Psi}_{m-1}| e^{iH_0 t/\hbar} P_z e^{-iH_0 t/\hbar}, \quad (12)$$

where $\tilde{\Psi}_0 \equiv \Phi_0$. Note that $\tilde{\Psi}_m$ contributes only to population of states coupled to the ground state by m -photon transitions. In particular, for a system initially prepared in $^1S^e$ symmetry, $\tilde{\Psi}_1$ is of $^1P^o$ symmetry whereas $\tilde{\Psi}_2$ contains states of both $^1S^e$ and $^1D^e$ symmetry (the superscripts “e” and “o” denote the parity of the states).

Now, for sufficiently weak laser pulses, the series in Eq. (9) converges rapidly. The sum over m can thus be truncated at a rather early stage without introducing any significant errors in $|\tilde{\Psi}\rangle$ or $\langle \tilde{\Psi}|$. We now choose $m \leq 2$ and adjust the parameters of the perturbation (i.e., of the laser pulses), to ensure that such a truncation is valid.

Using time-dependent perturbation theory we will now proceed to construct the wave function $\tilde{\Psi}$ and then compute the energy distribution of the system with the help of Eq. (5). This last step can be made with two alternative approaches, which both have advantages and disadvantages. This issue is best illustrated through a more detailed account of the calculation of the first-order term in the expansion.

A. First-order term

We note first that from Eq. (7) it follows that

$$\langle \Psi | \Phi(\epsilon) \rangle \langle \Phi(\epsilon) | \Psi \rangle = \langle \tilde{\Psi} | \Phi(\epsilon) \rangle \langle \Phi(\epsilon) | \tilde{\Psi} \rangle, \quad (13)$$

and thus the amplitudes needed in Eq. (2) to calculate $dP/d\epsilon$ can as well be expressed in terms of $\tilde{\Psi}$. With $m = 1$ in Eqs. (11) and (12), we write the first-order approximation of these amplitudes as

$$\langle \Phi(\epsilon) | \tilde{\Psi}_1 \rangle = -i2\pi \hat{A}(\epsilon - E_0) \langle \Phi(\epsilon) | P_z | \Phi_0 \rangle \quad (14)$$

$$\langle \tilde{\Psi}_1 | \Phi(\epsilon) \rangle = i2\pi \hat{A}(-(\epsilon - E_0)) \langle \Phi_0 | P_z | \Phi(\epsilon) \rangle, \quad (15)$$

where $\hat{A}(\Omega)$ is the Fourier transform of the vector potential, namely,

$$A(t) = \frac{1}{\hbar} \int_{-\infty}^{\infty} \hat{A}(\Omega) e^{-i\Omega t/\hbar} d\Omega, \quad (16)$$

and

$$\hat{A}(\Omega) \equiv \frac{1}{2\pi} \int_{-\infty}^{\infty} A(t) e^{i\Omega t/\hbar} dt. \quad (17)$$

The time integration over the factors $\exp[\mp i(\Omega_i \pm E_0 \mp \epsilon)t/\hbar]$ [cf. Eqs. (11) and (12)], gives now $\delta(E_0 - \epsilon + \Omega)$ and $\delta(\epsilon - E_0 + \Omega)$ in the calculations of Eqs. (14) and (15), respectively, and this determines the arguments of \hat{A} . With a real argument Ω , then $\hat{A}(-\Omega) = \hat{A}^*(\Omega)$, but here we have chosen to keep the notation $\hat{A}(-\Omega)$ for the use with complex scaling where the argument of \hat{A} is complex.

Combining Eqs. (14) and (15), we get finally the first-order approximation of the energy distribution of the system:

$$\begin{aligned} \frac{dP^1(\epsilon)}{d\epsilon} &= \langle \tilde{\Psi}_1 | \Phi(\epsilon) \rangle \langle \Phi(\epsilon) | \tilde{\Psi}_1 \rangle \\ &= 4\pi^2 \hat{A}(-(\epsilon - E_0)) \hat{A}(\epsilon - E_0) \\ &\quad \times \langle \Phi_0 | P_z | \Phi(\epsilon) \rangle \langle \Phi(\epsilon) | P_z | \Phi_0 \rangle. \end{aligned} \quad (18)$$

Now, let us turn to how the probability distribution can be computed with complex scaling. There are, at least, two alternatives. The first possibility is to follow Eq. (5) directly. $|\tilde{\Psi}_1^\theta\rangle$ and $\langle \tilde{\Psi}_1^\theta|$ are then constructed in the basis of H_0^θ and, following Eq. (18), we compute the numerator in Eq. (5) as

$$\begin{aligned} \langle \Psi_1^\theta | \Phi_n^\theta \rangle \langle \Phi_n^\theta | \Psi_1^\theta \rangle &= 4\pi^2 \hat{A}(-(E_n^\theta - E_0^\theta)) \hat{A}(E_n^\theta - E_0^\theta) \\ &\quad \times \langle \Phi_0^\theta | P_z e^{-i\theta} | \Phi_n^\theta \rangle \langle \Phi_n^\theta | P_z e^{-i\theta} | \Phi_0^\theta \rangle, \end{aligned} \quad (19)$$

and thus the energy distribution as

$$\begin{aligned} \frac{dP^1(\epsilon)}{d\epsilon} &= \text{Im} \left(\sum_n 4\pi \hat{A}(-(E_n^\theta - E_0^\theta)) \hat{A}(E_n^\theta - E_0^\theta) \right. \\ &\quad \left. \times \frac{\langle \Phi_0^\theta | P_z e^{-i\theta} | \Phi_n^\theta \rangle \langle \Phi_n^\theta | P_z e^{-i\theta} | \Phi_0^\theta \rangle}{E_n^\theta - \epsilon} \right), \end{aligned} \quad (20)$$

where we note that $E_0^\theta = E_0$. The advantage with this approach is that, once the expression in Eq. (19), which can be thought of as the generalized population in Φ_n^θ , is obtained for all n , then $dP^1/d\epsilon$ can easily be obtained for any ϵ . The drawback is that \hat{A} can grow very large for complex arguments.

A second alternative is to first calculate the Fourier transform in Eq. (18) for a real energy ϵ . After that one inserts the δ function, following the steps in Eqs. (2)–(4), and finally the transition to complex rotation is made; that is, Eq. (18) is instead transformed to

$$\begin{aligned} \frac{dP^1(\epsilon)}{d\epsilon} &= 4\pi \hat{A}(-(\epsilon - E_0)) \hat{A}(\epsilon - E_0) \\ &\quad \times \text{Im} \left(\sum_n \frac{\langle \Phi_0^\theta | P_z e^{-i\theta} | \Phi_n^\theta \rangle \langle \Phi_n^\theta | P_z e^{-i\theta} | \Phi_0^\theta \rangle}{E_n^\theta - \epsilon} \right). \end{aligned} \quad (21)$$

This second version [Eq. (21)] is in fact equivalent with approaches used earlier in the literature for absorption of monochromatic light [41,42]. The fact that the Fourier transformation of the vector potential can be calculated for real energies only is an advantage if \hat{A} is less well behaved for complex arguments. This is, for example, the case if $A(t)$ is a plane wave and thus $\hat{A}(\Omega)$ is a δ function. There is no drawback with Eq. (21) in first order, but in higher orders the same procedure, as will be discussed in Sec. III B below, leave us with a time-consuming integration over intermediate energies.

Before proceeding to the second-order term we note that in both Eqs. (20) and (21) the vector potential is just a factor before the atomic term. An A field that varies slowly over a resonance profile will thus not be able to affect its form. The situation is quite different when we consider the contributions from the second-order term.

B. Second-order term

Let us now turn to how the second-order contributions to the wave function affect $dP/d\epsilon$ [Eq. (2)]. For this the amplitudes $\langle\Phi(\epsilon)|\tilde{\Psi}_2\rangle$ and $\langle\tilde{\Psi}_2|\Phi(\epsilon)\rangle$ are needed. $\tilde{\Psi}_2$ is obtained from the $m = 2$ terms in Eqs. (11) and (12), which are due to two interactions with the electromagnetic field,

$$\Phi_0 \xrightarrow{\Omega_1} \tilde{\Psi}_1 \xrightarrow{\Omega_2} \tilde{\Psi}_2. \quad (22)$$

Let us first consider

$$\begin{aligned} \langle\Phi(\epsilon)|\tilde{\Psi}_2\rangle &= -2i\pi \sum_s \langle\Phi(\epsilon)|P_z|\Phi_s\rangle \langle\Phi_s|P_z|\Phi_0\rangle \\ &\times \int_{-\infty}^{\infty} \frac{\hat{A}(\epsilon - E_0 - \Omega_2)\hat{A}(\Omega_2)}{E_0 - E_s + \Omega_2 + i\epsilon} d\Omega_2, \end{aligned} \quad (23)$$

where again it is the time integrations that single out the energy-conserving process and ensure that $\epsilon - E_0 = \Omega_1 + \Omega_2$ and which further determine the arguments of \hat{A} (cf. Sec. III A). The imaginary constant $i\epsilon$ in the denominator moves the pole off the real energy axis and its sign is determined from the requirement that $\Psi_m(t) \rightarrow 0$, $t \rightarrow -\infty$ for $m > 0$ (i.e., that the system is in the ground state at $t \rightarrow -\infty$). In the integration over Ω_2 in Eq. (23) there are thus poles at $\Omega_2 = E_s - E_0 - i\epsilon$, and consequently the integration path (along the real axis) is above the poles.

Let us now consider complex rotation. The intermediate energies are now eigenstates to a complex rotated Hamiltonian and are in general complex with a negative imaginary part (i.e., $E_s \rightarrow E_s^\theta$). Hereby the poles will move, but just farther away from the real axis and the integration over Ω_2 will only be more stable numerically. Since this integration only involves the Fourier transform of the analytically known vector potential and an energy denominator, it is conveniently done, for example, with Gaussian quadrature.

The situation for $\langle\tilde{\Psi}_2|\Phi(\epsilon)\rangle$ is, however, different. The corresponding expression is

$$\begin{aligned} \langle\tilde{\Psi}_2|\Phi(\epsilon)\rangle &= 2i\pi \sum_s \langle\Phi_0|P_z|\Phi_s\rangle \langle\Phi_s|P_z|\Phi(\epsilon)\rangle \\ &\times \int_{-\infty}^{\infty} \frac{\hat{A}(-(\epsilon - E_0 - \Omega_2))\hat{A}(-\Omega_2)}{E_0 - E_s + \Omega_2 - i\epsilon} d\Omega_2, \end{aligned} \quad (24)$$

and here the poles are instead at $\Omega_2 = E_s - E_0 + i\epsilon$, and the Ω_2 integration along the real axis is below the poles. Now if $E_s \rightarrow E_s^\theta$ the poles would move to the lower complex plane and the Ω_2 integration would give a different result. To handle this situation we choose to replace the integration along the real axis with a path above the poles. This can be done as long as we take proper account of the pole contribution. We get then an alternative representation of Eq. (24):

$$\begin{aligned} \langle\tilde{\Psi}_2|\Phi(\epsilon)\rangle &= \sum_s \langle\Phi_0|P_z|\Phi_s\rangle \langle\Phi_s|P_z|\Phi(\epsilon)\rangle \\ &\times \left[-4\pi^2 \hat{A}(-(\epsilon - E_s))\hat{A}(-(E_s - E_0)) \right. \\ &\left. - i2\pi \int_{-\infty}^{\infty} \frac{\hat{A}(-(\epsilon - E_0 - \Omega_2))\hat{A}(-\Omega_2)}{E_0 - E_s + \Omega_2 + i\epsilon} d\Omega_2 \right]. \end{aligned} \quad (25)$$

Here we may again introduce complex scaling. In the second term the integration path will then again be automatically on the side of the poles indicated by $+i\epsilon$ and we may let $\epsilon \rightarrow 0^+$. The drawback is the necessity to compute the extra term contributed by the pole [i.e., the first term on the right-hand side of Eq. (25)].

Now we proceed as in Sec. III A and use Eq. (5) to replace $|\Phi(\epsilon)\rangle\langle\Phi(\epsilon)|$ with a finite sum of eigenstates to the complex rotated Hamiltonian. Again, as in Eqs. (20) and (21), there are two possible choices. The first version [cf. Eq. (20)] involves the calculation of \hat{A} with complex arguments, which on the other hand can be done once and for all due to the replacement of $|\Phi(\epsilon)\rangle\langle\Phi(\epsilon)|$ just mentioned. The second version [cf. Eq. (21)], requires the integration over Ω_2 for each desired energy ϵ , but \hat{A} is here less cumbersome to handle. In Eq. (23) the argument of \hat{A} is with this choice real and in Eq. (25) it is only in the pole contribution (the first term) that we encounter complex arguments of \hat{A} . The calculations presented below are generally done with the first, faster, version, but then a few energy points are calculated with the second version to check that we indeed get the same results. A rather modest complex scaling angle is sufficient to uncover the resonances of importance for the light pulses considered, and it has been checked for stability over the region $\theta = 2^\circ$ to 5° .

In both Eqs. (23) and (25) the vector potential is no longer just a prefactor. Through the integration over Ω_2 it has a direct influence on which intermediate states Φ_s , which are populated and thus the probability to reach a certain final state $\Phi(\epsilon)$. Here it is thus conceivable that the actual form of the light field should be able to influence the form of the resonance profile.

IV. REPRESENTATION OF FIELD-FREE STATES

Before turning to the results, we give a brief account of how the field-free states are represented. The same method has been used earlier for calculations of resonance parameters and photodetachment cross sections [44–48].

The complex rotated field-free Hamiltonian is

$$H_0 = h_1 + h_2 + \frac{e^2}{4\pi\epsilon_0 r_{12}} e^{-i\theta}, \quad (26)$$

with

$$h_i = \frac{\mathbf{p}_i^2}{2m} e^{-i2\theta} - \frac{e^2}{4\pi\epsilon_0 r_i} Z e^{-i\theta}. \quad (27)$$

The eigenstates to h are expanded in products of B splines [49] and spherical harmonics Y_ℓ^m ; that is, the radial functions $P_{n\ell}$ are written

$$P_{n\ell}(r e^{i\theta}) = \sum_i c_i B_i^k(r). \quad (28)$$

The B splines are piecewise polynomials of order $k - 1$ (here $k = 7$) defined on a so-called knot sequence. They form a finite basis that is complete on the space determined by the polynomial order and the knot sequence. The c_i s in Eq. (28) are obtained from a diagonalization of the one-particle Hamiltonian matrix in the B -spline basis. The B splines are kept real, and the rotational angle θ thus only affects the c_i coefficients. The knot sequence starts off linearly and extends out to 200–300 a.u., and the convergence with respect to the density of the grid and the size of the radial box is checked. For the outer region of the knot sequence a linear grid with larger steps, as well as an exponentially increasing grid, has been tested and both are found to be adequate. The two-particle Hamiltonian in Eq. (26) is finally diagonalized for a given symmetry and parity using that coupled eigenfunction to $h_1 + h_2$ as a basis; that is, with matrix elements

$$\langle \{n_a \ell_a n_b \ell_b\}_{LS}^\pi | H_0 | \{n_c \ell_c n_d \ell_d\}_{LS}^\pi \rangle. \quad (29)$$

We build the configurations from the full basis spanned by the chosen B splines and include $\ell \leq 2$ which is sufficient for stable resonance profiles. This has been checked through calculations with $\ell \leq 3$. The bottleneck in the present calculation is the extended and finely meshed knot sequence needed for the description of the energy distribution in the continuum. Already with the modest number of included partial waves of $\ell \leq 2$, the two-particle basis consists of up to $\sim 25\,000$ pairs of one-particle functions of $^1P^0$ symmetry as well as $\sim 19\,000$ pairs of $^1S^0$ symmetry. Still, even with $\ell \leq 2$, the resonance parameters are well represented. For example, the lowest 1S resonance (discussed below) is found at $-0.148\,766$ a.u., while the highly accurate parametric coordinate calculation in Ref. [50] places it at $-0.148\,776$ a.u. Similarly, the halfwidth found here is 8.693×10^{-4} a.u., while that of Ref. [50] is 8.666×10^{-4} a.u.

V. RESULTS

We consider a light pulse built from a sum of pulses with Gaussian envelopes:

$$A(t) = \sum_k A_k e^{-[(t-d_k)/T_k]^2} \sin[\omega_k(t-d_k)], \quad (30)$$

where a nonzero d_k yields possible delay of the term k . In the following T_k will be one light cycle (i.e., $T_k = 2\pi/\omega_k$). Longer pulses have been tested as well, but this did not give any qualitatively different results. The Fourier transform of the

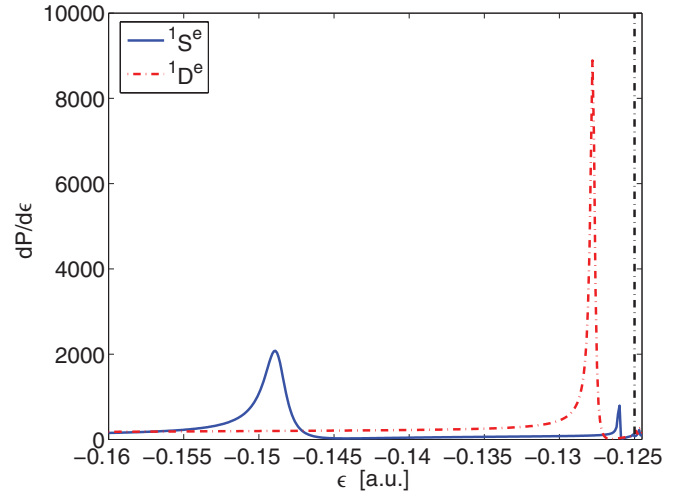


FIG. 1. (Color online) Overview of resonances that can be reached with two photons from the H⁻ ground state in the region just below the H($n = 2$) threshold. The $^1S^e$ channel is shown in blue (solid line) and the $^1D^e$ channel in red (dashed-dotted line). The vertical line at -0.125 a.u. shows the position of the H($n = 2$) threshold.

field in Eq. (30) is

$$\hat{A}(\Omega) = -\frac{i}{4\sqrt{\pi}} \sum_k A_k T_k e^{id_k\Omega/\hbar} \left\{ \exp\left[-\frac{T_k^2}{4}(\omega_k + \Omega/\hbar)^2\right] - \exp\left[-\frac{T_k^2}{4}(\omega_k - \Omega/\hbar)^2\right] \right\}. \quad (31)$$

The numerical results presented below have been obtained with fields composed of 1 or 2 terms in Eqs. (30) and (31).

Figure 1 shows an overview of the resonances reachable through two-photon absorption from the H⁻ ground state. The displayed region is just below the threshold for electron detachment accompanied by excitation of the remaining hydrogen atom into $n = 2$, situated at ~ 11 eV above the ground state. The spectrum is generated with the light pulse in Eq. (30) with just one term in the sum, and with $\hbar\omega_1 = 0.19$ a.u. (~ 5.2 eV). The duration of the pulse is around 2 fs. Since the first detachment threshold is found already at ~ 0.75 eV, absorption of one photon of this energy is more than enough to release one electron. The energy region then reached is also empty of resonances. The process addressed (i.e., that of absorbing more than the necessary number of photons) is for negative ions often called excess-photon detachment [36] and is an analog to above threshold ionization for atoms.

As can be seen in Fig. 1, the lowest energy H⁻ resonance is broad, strong, and rather isolated. It will here serve as a test example for how a resonance profile can be modified by the pulses used to excite it. The resonance is of $^1S^e$ symmetry and its precise position is ~ 10.3068 eV above the ground state, which means that its total energy with respect to three-particle breakup is $-0.148\,776$ a.u., and it has a halfwidth of $0.000\,866\,6$ a.u. (~ 24 meV) [50].

A light pulse built from two terms in Eq. (30) has now been used to excite the lowest $^1S^e$ resonance. The carrier frequencies are chosen such that $\hbar(\omega_1 \pm \omega_2)$ equals the excitation energy of the $^1S^e$ resonance. An example of a considered light field is shown in Fig. 2. In this example, absorption of the central

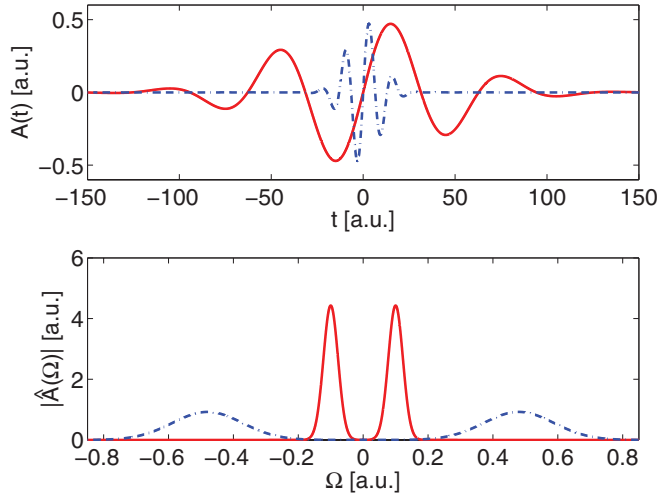


FIG. 2. (Color online) Example of a vector potential used in the present calculations. The upper panel shows the two pulses as a function of time. The lower panel shows the Fourier transform of the A field. The pulses are chosen such that absorption and/or emission of photons corresponding to the energy of the central frequencies of both pulses match the excitation energy of the $1S^e$ resonance. In this example absorption of the central frequency of the higher-energy pulse (blue dashed-dotted line), corresponding to ~ 13 eV is sufficient to reach the $H(n=3)$ threshold, at ~ 12.8 eV. Through subsequent emission of a photon with an energy corresponding to the central frequency of the lower-energy pulse (solid red line) the $1S$ resonance, at ~ 10.3 eV, can be populated.

frequency of the higher-energy pulse (blue), corresponding to ~ 13.1 eV will bring the system all the way to the region around the $H(n=3)$ threshold (at ~ 12.8 eV), and thus well above the $1S^e$ resonance at ~ 10.3 eV. Through subsequent emission of a photon with an energy corresponding to the central frequency of the lower-energy pulse (red) the $1S$ resonance can be populated. In contrast to the region above the first ionization threshold, the region between the second and third ionization threshold shows a number of resonances. The taken path is also illustrated by the two rightmost arrows in Fig. 3.

Figure 4 shows first the energy distribution in the vicinity of the $1S^e$ resonance after the ion has been exposed to a light field consisting of one pulse (or equivalently two equal superimposed pulses) with a central frequency matching half the needed excitation energy (0.19 a.u. ≈ 5.2 eV). The path is illustrated by the leftmost arrows in Fig. 3. Since detachment is only possible into the $1s\epsilon$ channel, the figure can be reinterpreted as the photoelectron spectrum by just shifting the x axis with 0.5 a.u. The amplitude of the A field is, for simplicity, set to unity, as can be seen in the lower panel, and $dP/d\epsilon$ for any other amplitude is obtained by multiplication of the curve in the upper panel in Fig. 4 with the fourth power of the amplitude. In Fig. 5 the situation is instead one pulse with a central frequency corresponding to 0.10 a.u. ≈ 2.7 eV and one more energetic pulse with a central frequency corresponding to 0.28 a.u. ≈ 7.6 eV; that is, the path illustrated by the two middle arrows in Fig. 3. Figure 6 shows the opposite situation; a more energetic pulse with a central frequency corresponding to 0.48 a.u. ≈ 13.1 eV and again one pulse with a central frequency corresponding to 0.10 a.u. ≈ 2.7 eV, this was the

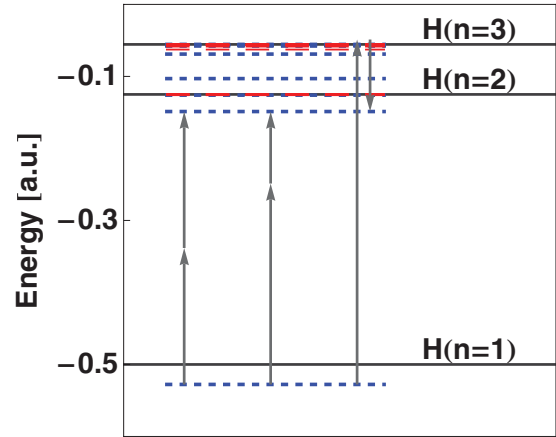


FIG. 3. (Color online) Energy-level diagram of H^- showing ground state and resonances of $1S$ and $1P$ symmetry up to the $H(n=3)$ threshold. States of even $1S$ symmetry are shown with blue short dashed lines and those of odd $1P$ symmetry with red long dashed lines. The arrows show the central frequencies of the three different investigated light pulses.

case discussed in connection with Fig. 2. In Figs. 5 and 6 the amplitudes A_1 and A_2 [cf. Eq. (30)] are equal and half an atomic unit each, which corresponds to the situation in Fig. 4 if we view it as the field from two equal superimposed pulses.

Comparing the profiles, as is done in Fig. 7, we see that the peak asymmetry changes and a careful examination will also show that there is a slight change of peak position, where the example in Fig. 5 has its peak for a slightly lower energy than in Fig. 4, while that in Fig. 6 is slightly higher. For easy comparison the magnitude of the vector-potentials has been adjusted in Fig. 7 so that the resonance peaks have the same height in all three cases.

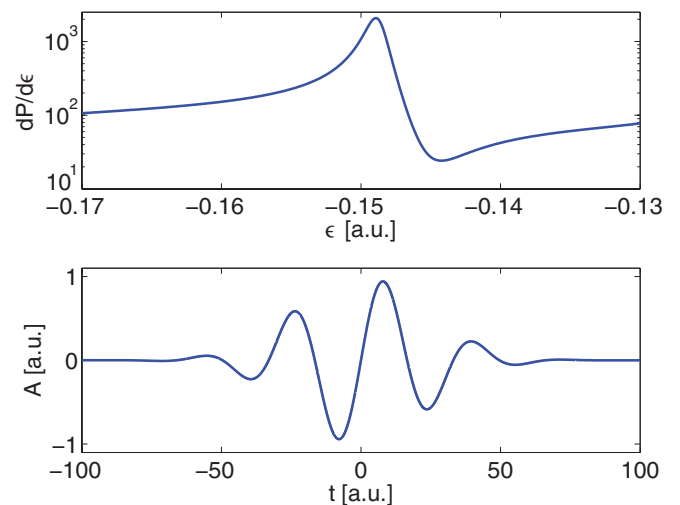


FIG. 4. (Color online) Upper panel shows the energy distribution in the vicinity of the $1S^e$ resonance after exposure to a light field consisting of two equal pulses, each with a central frequency half the needed excitation energy (0.19 a.u. ≈ 5.2 eV). Lower panel shows the vector potential.

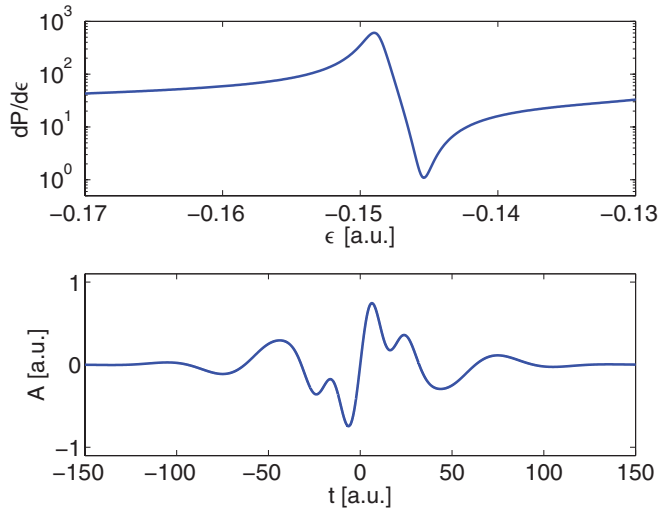


FIG. 5. (Color online) Upper panel shows the energy distribution in the vicinity of the $1S^e$ resonance after exposure to a light field consisting of one pulse with a central frequency corresponding to 0.10 a.u. \approx 2.7 eV, and one with a central frequency corresponding to 0.28 a.u. \approx 7.6 eV. Lower panel shows the vector potential.

The asymmetry can be altered further by letting $\hbar\omega_1 + \hbar\omega_2$ be slightly different than the energy needed to reach the resonance. If the sum is not too much different the total population of the resonance is still only modestly affected. It should be possible to optimize the pulse for maximum asymmetry with some optimal control scheme, but we have not pursued this path here.

All the results shown are calculated with the two Gaussian pulses superimposed in time [i.e., $d_1 = d_2 = 0$ in Eq. (30)]. The procedure works equally well with a delay between the pulses. However, this leads to a much reduced population of the resonance and we have not investigated this further.

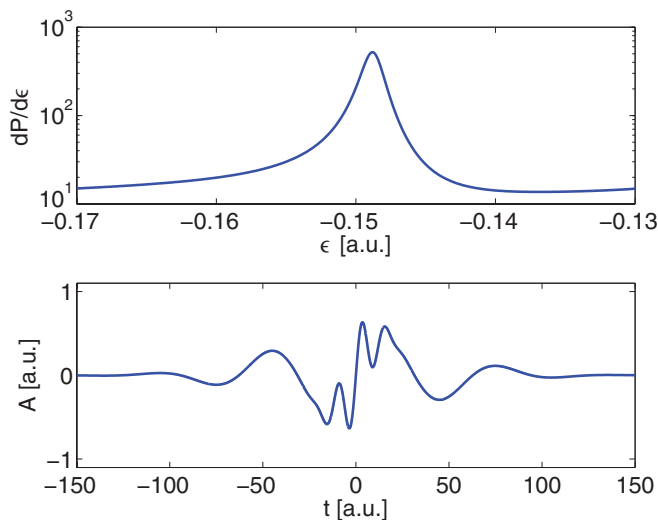


FIG. 6. (Color online) Upper panel shows the energy distribution in the vicinity of the $1S^e$ resonance after exposure to a light field consisting of one pulse with a central frequency corresponding to 0.48 a.u. \approx 13.1 eV, and one with a central frequency corresponding to 0.10 a.u. \approx 2.7 eV. Lower panel shows the vector potential.

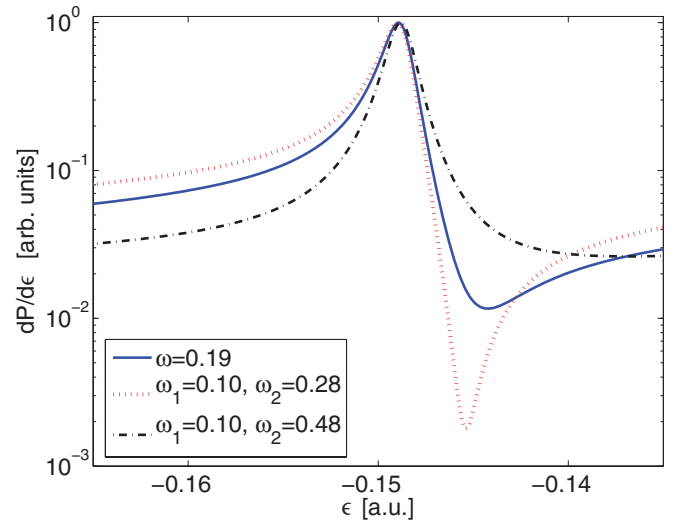


FIG. 7. (Color online) Comparison between energy distributions in vicinity of the $1S^e$ resonance at ~ -0.15 a.u. for different light pulses. The three profiles are normalized to the same maximum height to facilitate comparison.

A. Asymmetry parameter

Resonance profiles are often characterized by the asymmetry parameter q of the Fano profile [29]:

$$\frac{dP(\epsilon)}{d\epsilon} = c_0 + c_1 \frac{(\eta + q)^2}{1 + \eta^2}, \quad \text{with } \eta = \frac{(\epsilon - E_{\text{res}})}{\Gamma/2}, \quad (32)$$

where c_0 and c_1 are constants. E_{res} and Γ are the position and width of the resonance, respectively, and η is thus a dimensionless parameter normalized to the resonance width. This form was originally derived by Fano for one-photon absorption, but it is easy to show that it follows directly from Eq. (5). Looking at the contribution from one single resonance, we find, after introduction of the parameter η , that it can be

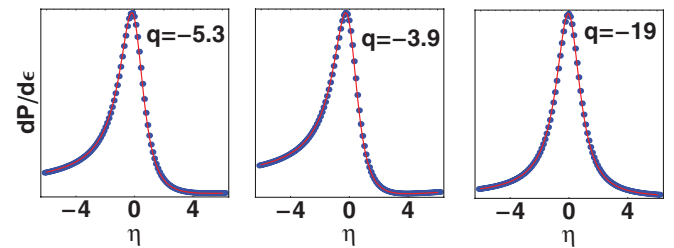


FIG. 8. (Color online) Fano profile fits [cf. Eq. (32)] of the resonance profile when excited with different light pulses. The blue dots show the calculated points and the red lines are the fits. The left panel shows the profile after excitation with one pulse where the central frequency matches half of the excitation energy (cf. Fig. 4). The middle panel shows the profile after excitation with two pulses centered at different frequencies, both tuned below the excitation energy (cf. Fig. 5), and the right panel shows the profile when the frequency of one of the pulses is tuned above the excitation energy (cf. Fig. 6). The dimensionless parameter η , as well as the asymmetry parameter q , are defined in Eq. (32). The three profiles are normalized to the same height.

written as in Eq. (32) with

$$q = -\chi \pm \sqrt{\chi^2 + 1}, \quad (33)$$

where χ is the ratio between the real and the imaginary part of the generalized population of the resonance:

$$\chi = \frac{\text{Re}[\langle \Psi^\theta | \Phi_n^\theta \rangle \langle \Phi_n^\theta | \Psi^\theta \rangle]}{\text{Im}[\langle \Psi^\theta | \Phi_n^\theta \rangle \langle \Phi_n^\theta | \Psi^\theta \rangle]}. \quad (34)$$

The + and – in Eq. (33) are to be used if $\text{Im}[\langle \Psi^\theta | \Phi_n^\theta \rangle \langle \Phi_n^\theta | \Psi^\theta \rangle]$ is greater or smaller than zero, respectively. Eq. (32) is thus equally valid for multiphoton absorption.

The profiles calculated with the different light pulses are fit to Eq. (32) and displayed in Fig. 8 together with the q values calculated with Eq. (33). The q values obtained from the fit agree to within one unit in the last digit with the calculated ones. Asymmetry parameters close to zero imply strong asymmetry, while a close-to-Lorentzian profile has a large absolute q value. It is interesting to note that, for the case where the central frequency of one pulse is tuned well above the resonance (the right panel in Fig. 8), the profile is close to Lorentzian with a much large magnitude of the q value than in the other two cases. The middle panel shows, on the other hand, a stronger asymmetry than what is obtained with one single pulse. The maximum of a Fano profile is

found at $\eta = 1/q$ (i.e., at $\epsilon = E_{\text{res}} + \Gamma/2q$), and the negative q values are thus consistent with lower-energy peaks for the more asymmetric profiles. The minimum, found at $\eta = -q$ (i.e., at $\epsilon = E_{\text{res}} - q\Gamma/2$) is perhaps more interesting. It is for the most asymmetric case found ~ 100 meV above the resonance position, but ~ 450 meV above it in the most symmetric case.

VI. CONCLUSIONS

We have combined complex rotation with time-dependent perturbation theory and used the developed formalism to study the interaction of a strongly correlated system with short light pulses. Corrections up to second order in the perturbing light field was included in the wave function.

The explicit representation of resonance states provided by complex scaling was decisive to keep the calculation within reach for a modest table-top computer. We showed further that, with two light pulses, we can steer the ionization path which is manifested in a change in the line profiles.

ACKNOWLEDGMENTS

Financial support from Göran Gustafsson Foundation and the Swedish Research council (V.R.) is gratefully acknowledged.

-
- [1] A. J. F. Siegert, *Phys. Rev.* **56**, 750 (1939).
 [2] J. Aguilar and J. Combes, *Commun. Math. Phys.* **22**, 269 (1971).
 [3] E. Balslev and J. Combes, *Commun. Math. Phys.* **22**, 280 (1971).
 [4] B. Simon, *Commun. Math. Phys.* **27**, 1 (1972).
 [5] B. Simon, *Ann. Math.* **97**, 247 (1973).
 [6] G. D. Doolen, J. Nuttall, and R. W. Stagat, *Phys. Rev. A* **10**, 1612 (1974).
 [7] Y. K. Ho, *J. Phys. B* **10**, L373 (1977).
 [8] Y. K. Ho, *J. Phys. B* **12**, 387 (1979).
 [9] K. T. Chung and B. F. Davis, *Phys. Rev. A* **26**, 3278 (1982).
 [10] Y. K. Ho, *Phys. Rev. A* **48**, 3598 (1993).
 [11] D. Wintgen and D. Delande, *J. Phys. B* **26**, L399 (1993).
 [12] A. Bürgers, D. Wintgen, and J.-M. Rost, *J. Phys. B* **28**, 3163 (1995).
 [13] E. Lindroth, *Phys. Rev. A* **49**, 4473 (1994).
 [14] D. R. DeWitt, E. Lindroth, R. Schuch, H. Gao, T. Quinteros, and W. Zong, *J. Phys. B* **28**, L147 (1995).
 [15] E. Lindroth and A.-M. Mårtensson-Pendrill, *Phys. Rev. A* **53**, 3151 (1996).
 [16] S. Berkovic, R. Krivec, V. Mandelzweig, and L. Stotland, *Phys. Rev. A* **55**, 988 (1997).
 [17] D. Nikolic and E. Lindroth, *J. Phys. B* **37**, L285 (2004).
 [18] J. Bengtsson, E. Lindroth, and S. Selstø, *Phys. Rev. A* **78**, 032502 (2008).
 [19] J. Bengtsson, E. Lindroth, and S. Selstø, *Phys. Rev. A* **85**, 013419 (2012).
 [20] M. Drescher, M. Hentschel, R. K. M. Uiberacker, V. Yakovlev, A. Scrinzi, Th. Westerwalbesloh, U. Kleineberg, U. Heinzmann, and F. Krausz, *Nature (London)* **419**, 803 (2002).
 [21] E. Goulielmakis, M. Uiberacker, R. Kienberger, A. Baltuska, V. Yakovlev, A. Scrinzi, T. Westerwalbesloh, U. Kleineberg, U. Heinzmann, M. Drescher, and F. Krausz, *Science* **305**, 1267 (2004).
 [22] J. Mauritsson *et al.*, *Phys. Rev. Lett.* **105**, 053001 (2010).
 [23] V. Vénierard, R. Taïeb, and A. Maquet, *Phys. Rev. A* **54**, 721 (1996).
 [24] A. K. Kazansky and N. M. Kabachnik, *J. Phys. B* **40**, 3413 (2007).
 [25] L. Argenti and E. Lindroth, *Phys. Rev. Lett.* **105**, 053002 (2010).
 [26] L. Moore, M. Lysaght, L. Nikolopoulos, J. Parker, H. van der Hart, and K. Taylor, *J. Mod. Opt.* **58**, 1132 (2011).
 [27] L. R. Moore, M. A. Lysaght, J. S. Parker, H. W. van der Hart, and K. T. Taylor, *Phys. Rev. A* **84**, 061404 (2011).
 [28] J. S. Parker, L. R. Moore, K. J. Meharg, D. Dundas, and K. T. Taylor, *J. Phys. B* **34**, L69 (2001).
 [29] U. Fano, *Phys. Rev.* **124**, 1866 (1961).
 [30] A. E. Miroshnichenko, S. Flach, and Y. S. Kivshar, *Rev. Mod. Phys.* **82**, 2257 (2010).
 [31] V. Vargiamidis, V. Fessatidis, and N. J. M. Horing, *J. Appl. Phys.* **106**, 043710 (2009).
 [32] R. A. Vicencio, J. Brand, and S. Flach, *Phys. Rev. Lett.* **98**, 184102 (2007).
 [33] P. Balling, H. H. Andersen, C. A. Brodie, U. V. Pedersen, V. V. Petrunin, M. K. Raarup, P. Steiner, and T. Andersen, *Phys. Rev. A* **61**, 022702 (2000).
 [34] P. Balling, M. K. Raarup, U. V. Elstrøm, R. Martinussen, V. V. Petrunin, and T. Andersen, *Phys. Rev. A* **76**, 044701 (2007).
 [35] A. Stintz, X. M. Zhao, C. E. M. Strauss, W. B. Ingalls, G. A. Kyrála, D. J. Funk, and H. C. Bryant, *Phys. Rev. Lett.* **75**, 2924 (1995).
 [36] D. C. Rislove, C. E. M. Strauss, H. C. Bryant, M. S. Gulley, D. J. Funk, X. M. Zhao, and W. A. Miller, *Phys. Rev. A* **58**, 1889 (1998).
 [37] D. Proulx, M. Pont, and R. Shakeshaft, *Phys. Rev. A* **49**, 1208 (1994).
 [38] H. W. van der Hart, *Phys. Rev. A* **50**, 2508 (1994).

- [39] I. Sánchez, H. Bachau, and F. Martín, *J. Phys. B* **30**, 2417 (1997).
- [40] N. Moiseyev, P. R. Certain, and F. Weinhold, *Mol. Phys.* **36**, 1613 (1978).
- [41] T. N. Rescigno and V. McKoy, *Phys. Rev. A* **12**, 522 (1975).
- [42] E. Lindroth, *Phys. Rev. A* **52**, 2737 (1995).
- [43] J. J. Sakurai, *Modern Quantum Mechanics*, rev. ed. (Addison-Wesley Publishing Company, Boston, 1994), p. 325.
- [44] N. Brandefelt and E. Lindroth, *Phys. Rev. A* **59**, 2691 (1999).
- [45] N. Brandefelt and E. Lindroth, *Phys. Rev. A* **65**, 032503 (2002).
- [46] J. L. Sanz-Vicario, E. Lindroth, and N. Brandefelt, *Phys. Rev. A* **66**, 052713 (2002).
- [47] E. Lindroth, J. Wallenius, and S. Jonsell, *Phys. Rev. A* **68**, 032502 (2003).
- [48] M. Genkin and E. Lindroth, *Eur. Phys. J. D* **51**, 205 (2009).
- [49] C. deBoor, *A Practical Guide to Splines* (Springer-Verlag, New York, 1978).
- [50] A. Bürgers and E. Lindroth, *Eur. Phys. J. D* **10**, 327 (2000).